Available online at www.sciencedirect.com
ScienceDirect
Procedia Engineering 6 (2010) 153–162
Procedia Engineering
www.elsevier.com/locate/procedia

IUTAM Symposium on Computational Aero-Acoustics
for Aircraft Noise Prediction

Assessment of a frequency-domain linearised Euler solver for turbofan aft radiation predictions and comparison with measurements

Yusuf Özyörük[a,*] and Brian J. Tester[b]

[a]*Department of Aerospace Engineering, Middle East Technical University, Ankara, 06531, Turkey*
[b]*Institute for Sound and Vibration, University of Southampton, Southampton, SO 1BJ, UK*

Abstract

This paper presents a frequency-domain computational aeroacoustics tool for predicting aft noise radiation through turbofan ducts and jets and its application to two realistic engine exhaust configurations which have been experimentally tested. The tool is based on the discretised axisymmetric form of the linearised Euler equations in conjunction with perfectly matched layer equations at the inlet and far-field boundaries using high-order finite differences. The resultant linear system of equations is inverted by the state-of-the-art parallel sparse solver MUMPS. The far-field prediction is carried out by integrating Kirchhoff's formula in frequency domain. The code has already been verified extensively for idealized semi-infinite duct cases with comparisons to available analytical solutions with very good agreement. Therefore, we concentrate in this paper on numerical solutions to the experimental cases tested in the EC FP6 Project TURNEX (TUrbomachinery noise Radiated through the engine EXhaust) to assess and partially validate the present solver further. Comparisons of the computed results with the measured data reveal that the solver predicts the general noise radiation patterns and sound levels reasonably well, so long as the target in-duct azimuthal mode remains dominant as it radiates to the far-field. The agreement strongly suggests that, at least for the range of mean flows and acoustic conditions considered, the physical aeroacoustic radiation processes are fully captured through the frequency-domain solutions to the linearised Euler equations. © 2009 Published by Elsevier Ltd.

Keywords: computational aeroacoustics; linearized Euler equations; frequency-domain; convective instabilities; exhaust radiation.

1. Introduction

Aft radiation of turbomachinery noise occurs through bypass and core nozzle flows and jets. The effects of these flows on the propagating sound can be accounted for by solving the linearised Euler equations (LEE). Temporal solution of these equations, however, renders appearance of convective instabilities [1] and their indefinite growth in time [2], if not controlled by some artificial approach, such as filtering [3] and/or removing the flow gradients from the equations [4-7]. However, direct frequency-domain solutions filter out the temporally unstable modes [2]. Therefore, computational aeroacoustics (CAA) codes to perform such solutions have been developed recently [8-10]. Among these is the direct solver called FLESTURN [9,10]. It is a code developed within framework of the European Commission sponsored project TURNEX (TUrbomachinery noise Radiating through the engine EXhaust). This code solves the LEE directly in frequency domain on structured meshes employing the state-of-the-art

1877-7058
doi:10.1016/j.proeng.2010.09.017

MUMPS sparse linear system of equations solver [11,12]. Analytical solutions to the Munt problem [13] are available [14,15], and FLESTURN has already been extensively verified by solving idealized radiation problems from simple semi-infinite circular ducts and annular ducts with semi-infinite centerbodies, the latter being with both lined and hard walls. The computed results were compared with the analytical solutions of Demir and Rienstra [15] with very good agreement [9,10]. It is the purpose of this paper to assess and validate FLESTURN further by computing the experimental cases of the TURNEX project. These include a short and a long cowl experimental model at flow and zero flow conditions and at various frequencies. The flow conditions correspond typically to the three aircraft/engine operating conditions of approach, cutback, and sideline, all at a 'static' condition, i.e. without a flight stream, but no computations are presented for the sideline condition.

In the following sections, FLESTURN will be described briefly, which will be followed by a description of the experimental cases. Then, FLESTURN computations will be presented in comparison with the TURNEX data, with concluding remarks at the end.

2. Frequency-Domain Linearized Euler solver, FLESTURN

FLESTURN solves the LEE in the interior and perfectly matched layer (PML) equations [16] at in-duct and far-field boundaries of the domain as depicted in Figure 1. A structured mesh approach is used. On acoustically treated parts of the walls, the impedance boundary condition [17] is applied. All the equations are solved in the axial and radial coordinates by treating the azimuthal variation as periodic by the azimuthal mode order m. The physical structured mesh is mapped to a uniform computational mesh by the mappings $x=x(\xi,\eta)$, $r=r(\xi,\eta)$. Then both the LEE and PML equations are written in the same form as,

$$(i\omega+im)\,[\mathbf{I}]\,\mathbf{q} + [\mathbf{A}]\,\mathbf{q}_\xi + [\mathbf{B}]\,\mathbf{q}_\eta + [\mathbf{C}]\,\mathbf{q} = \mathbf{r}$$

where i is imaginary unit, ω is the circular frequency, [**I**] is the identity matrix, **q** is the solution vector, [**A**] and [**B**] are the Jacobean tensors that involve mean flow related terms transformed into the computational domain, [**C**] is the source tensor that involves gradients of the mean flow for the LEE and damping terms for the PML equations, as well as the sources due to these equations being formulated in cylindrical-polar coordinates. The right-hand side vector **r** contains the incident sound source related terms that are obtained by applying the PML equations to the reflected wave components in a layer at the duct inlets. Solid wall and liner impedance conditions are also treated by the above general form of the equations so that a unified assembly procedure for the discrete form of the equations is possible. The discrete set of the equations is written in the form

$$\mathbf{[CM]\,Q = R},$$

where **[CM]** is the global coefficient matrix, **Q** is the global solution vector, and **R** is the global right-hand side vector. The coefficient matrix is sparse in nature and therefore, the linear system of equations is solved using the state-of-the-art sparse system solver MUMPS [11,12].

In this paper the TURNEX experimental cases are computed using the standard 4^{th}-order finite difference scheme. The computational stencil for this scheme has 5 points in each of the grid lines, and the corresponding structure of the sparse coefficient matrix **[CM]** for a structured mesh has 5 non-zero entry bands, whereas 2 additional bands away from the diagonal would take place for a 7-point stencil, such as that of the DRP scheme [18]. Although such schemes were explored in development of FLESTURN, solutions of realistic problems became prohibitive due to significant increase in the bandwidth of the coefficient matrix, and the standard 4^{th}-order finite difference algorithm was found to yield results at lowered computational memory.

The far-field is computed through a surface integration over an open Kirchhoff surface constructed outside the bypass jet stream. In cases of no flow, the Kirchhoff surface is closed downstream.

More details about the FLESTURN code can be found in Refs. [9,10].

3. Experiments

The TURNEX experimental work at QinetiQ included measurements of radiation from two different exhaust models, one simulating a ¾ short cowl (Fig. 3a) and the other simulating a long cowl (buried nozzle) engine exhaust (Fig. 3b). A mode synthesizer was used to excite the target azimuthal mode *m* with all cut-on radial modes well upstream in the uniform annular section of the models (Fig. 3a-b). Phases and amplitudes (complex amplitudes) of the individual modes were measured downstream of the mode synthesizer but still in the uniform section just upstream of the realistic non-uniform section. The far-field sound pressures were measured with an azimuthal far-field array (FFA) and a polar microphone array (Fig. 4). The mode synthesizer was developed and operated by EADS Innovation Works for these experiments, while both in-duct and far-field measurements were performed by German Aerospace Center (DLR) [19,20].

The FFA data was specifically acquired to ensure that the target mode generated by the mode synthesizer was dominant in the far-field, and could therefore, be sensibly compared with the single azimuthal mode numerical CAA solutions, as in the present paper. However, the measured azimuthal spectra showed at some test points that levels of other modes exceeded that of the target mode. The reason for this was concluded as either the flow inside the nozzle or the jet flow caused asymmetric variations of the radiated pattern after a detailed analysis performed by DLR on the measured data [20].

For validation purposes of the present CAA model test points were selected such that the measured target mode level was not significantly lower than the other mode levels, but the numerical solutions in this paper are compared with the 'overall' FFA measured tone levels (not the target azimuthal mode level) as well as tone levels measured with the polar microphone array.

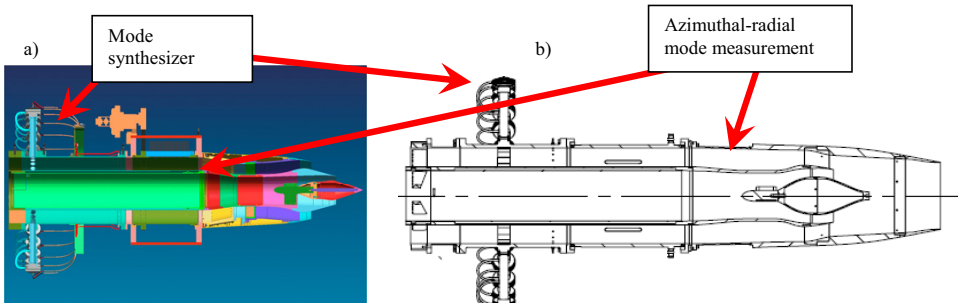

Figure 3: a) Short cowl, and b) long cowl model engine exhausts tested at QinetiQ.

Figure 4: Far-field azimuthal mode measurement (FFA) + polar measurement (SPL) at QinetiQ facility.

4. Computational results and discussion

4.1. Short cowl configuration

Measurements were taken at three different mean flow conditions, as well as without flow. The three flow conditions included both primary (core) and secondary (bypass) streams, but no external (flight) stream. The flow conditions corresponded typically to the three aircraft/engine operating conditions of approach, cutback, and sideline, all at a 'static' condition, i.e. without a flight stream. The corresponding mean flows were computed using the commercial CFD code Fluent using the k-epsilon turbulence model.

All acoustic calculations were carried out for unit pressure amplitude and zero phase for each individual, incident hardwall radial mode. The solutions for all the cut-on radial modes were then combined with the correct phase and amplitude information obtained from the in-duct measurements. Table 1 summarizes the computed short cowl cases. Specifically the flow conditions, frequencies, azimuthal mode orders, and the corresponding number of cut-on radial modes are shown. In the table the difference between the target mode level and the highest level among the others, defined as the target versus achieved (TVA) level in the experiments, is also shown for each acoustic case. A high value for TVA indicates a well achieved target mode by the mode synthesizer in the duct.

Table 1: Short cowl acoustic cases.

Short cowl case 5	**TP**	**Freq, Hz**	***m***	**#radial modes**	**TVA, dB**
No flow	21	4537.5	0	2	12.8
	23	4537.5	7	2	12.6
Static approach	1	4056.25	0	2	20.3
	6	8503.75	10	3	15.8
Static cutback	10	3810	8	1	8.9

Acoustic computations at zero flow were performed and compared with experimental data for azimuthal mode orders of m=0 and m=7 at 4537.5 Hz. The corresponding TVA levels to these modes were 12.8 and 12.6 dB, respectively (Table 1). These values indicate the two modes were produced reasonably well in the duct. The results were obtained on a mesh with 1225×23 nodal points for the core stream block (see Fig. 1), 1723×43 points for the bypass stream block, and 1525×231 points for the external stream block. Far-field pressures were calculated using a Kirchhoff surface enclosing the entire nozzle exit due to absence of jet flow. Comparison of the predicted far-field sound pressure levels (SPL) with the measured data for the m=0 mode is shown in Fig. 6a. The main lobe was predicted to lie along the cowl axis where no data was measured. The reason for the large discrepancies at the small angles might be due to weak reflections of this main lobe, since its level on axis is some 20 dB above that at 35^o. The computed SPLs agree reasonably well with the FFA data above about 35^o, and there are about 5 dB differences between the predicted levels and the polar array data for most angles. The only other possible cause for the differences in the zero flow case might be attributable to contributions from the non-target modes to the far-field levels, despite the in-duct dominance of the target mode. This should be verified by further investigation. Comparisons generally improve though for zero flow when the azimuthal mode number is increased while keeping the frequency at 4537.5 Hz. Fig. 6b shows the comparison for the m=7 mode. It is evident that the predicted levels agree with the experimental data quite well.

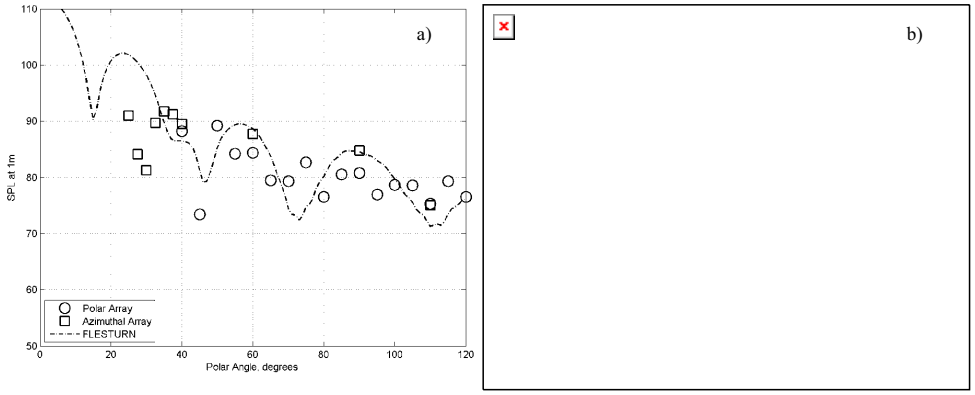

Figure 6: Far-field SPL distribution for a) m=0, b) m=7 mode at f=4537.5 Hz, zero flow (2 radial modes cut-on).

Figure 7a shows the computed pressure field radiated from the short cowl configuration at the static approach condition by the first radial mode of the m=10 target mode at 8503 Hz. This mode was excited with a TVA level of 15.8 dB. The same mesh as that of the zero flow case was used. Since here flow was involved, the effects of the mesh resolution and Kirchhoff surface placement on the computed results were studied. However, due to space limitations results pertaining to these studies are not shown. It was found that the chosen Kirchhoff surface and the used mesh resolution were sufficient. The computed far-field SPL distributions contributed by all the cut-on radial modes are compared with the measured data in Fig. 7b. Reasonably good agreement is observed in this comparison.

It may be useful at this point to note that as evident from Fig. 7a no convective spatial instability waves occurred along the shear layer trailing the cowl lip at this frequency, although the LEE support them, as will be seen for lower frequencies in the subsequent discussions. A momentum thickness (θ) analysis based on the RANS computed shear layer near the nozzle exit revealed that at this frequency the Strouhal number $\omega\theta/U_j$ as defined by Michalke [1] was near 0.29, which fell outside the unstable range[a] according to his stability analysis for round, incompressible free jets of similar profile.

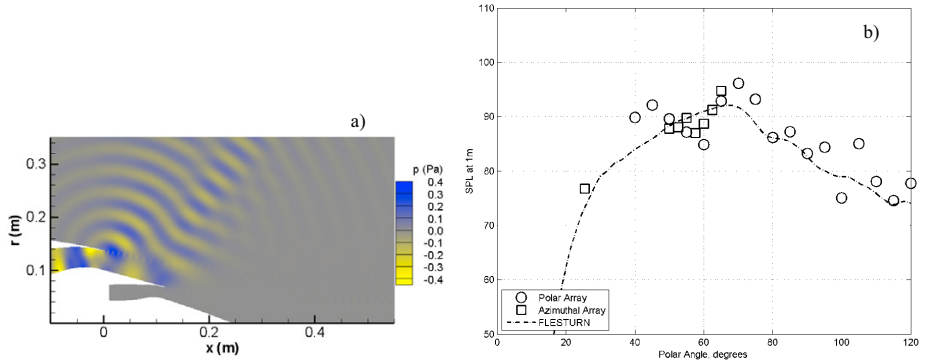

Figure 7: a) Pressure field for the (10,1) mode at f=8503 Hz, static approach, b) far-field SPL (3 rad. modes).

[a] This range was given in [1] for $m = 0$, and here we are using this range for $m = 10$ mode as a crude approximation.

As opposed to the preceding case, when the frequency was lowered to f=4056.25 Hz and the m=0 target mode was run at the static approach flow condition, an instability appeared along the shear layer starting at the cowl lip as shown in Fig. 8a. Along with determining the variation of the momentum thickness based Strouhal number, which is presented graphically in Fig. 8b, a close look into this region revealed that the axial velocity of the bypass stream outside the shear layer remained nearly constant at U_j=150 m/s, while the axial distance, λ, from one peak to the next in the train of instability waves marked in Fig. 8a varied as shown in Table 2 below. The corresponding phase velocities were approximated simply by λ f, yielding the values given in the table. In order to assess whether these waves were in fact associated with Kelvin-Helmholtz (K-H) instability, the values of their phase speed were approximated by (2/3)U_j along the jet. The evaluated values based on the local jet speed U_j are also included in the table. These values and the post-processed λ f values from Fig. 8a turned out to be sufficiently close in the early stages of the instability, where the momentum thickness is rather low (Fig. 8b), and the (2/3)U_j approximation is reasonable for round jets [1,21]. Also, Michalke's Strouhal number was calculated to be nearly 0.17 just downstream of the nozzle exit. This value was in the unstable region as shown in Fig. 8b. As the jet spreads, the momentum thickness and the phase velocity increase but the growth rate decreases and eventually the instability disappears, as was also the case for the computed results. It is also known that K-H instability arises due to the flow gradients. Therefore, we repeated the solution by employing the so-called gradient term suppression (GTS) approach in FLESTURN, similar to the work of Ref. [4]. In this case the instability disappeared totally as shown in Fig. 9a. By comparing the radiation patterns given in Fig. 8a and 9a, we observe that the acoustic waves for this case do not have significant interaction with the instability waves. Hence, despite the dominance of the pressure associated with the instability, the far-field SPLs were predicted well, as shown in the comparison with the measured data in 9b. For this test point the measured TVA level was 20.3 dB, showing a well achieved target mode. The computations confirm this for a wide range of angles as shown in the comparison.

Table 2: Parameters along shear layer between bypass stream and ambient air at 4056 Hz, m=0, static approach.

Parameter / Station #	1	2	3	4	5
x (m)	0.0594	0.0837	0.1087	0.1358	0.1643
λ = Δx (m)	-	0.0243	0.0250	0.0271	0.0285
U_j (m/s)	150.8	150.5	150.2	149.4	149.8
λ f (m/s) [f=4056 Hz]	-	**98.6**	**101.4**	109.9	115.6
(2/3)U_j (m/s)	100.5	**100.3**	**100.1**		

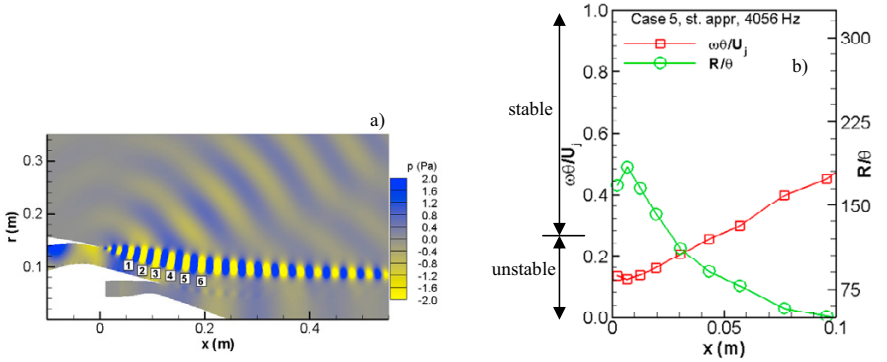

Figure 8: a) Pressure field for the m=0, n=1 mode at static approach, f=4056.25 Hz, b) Strouhal number variation along the shear layer based on momentum thickness.

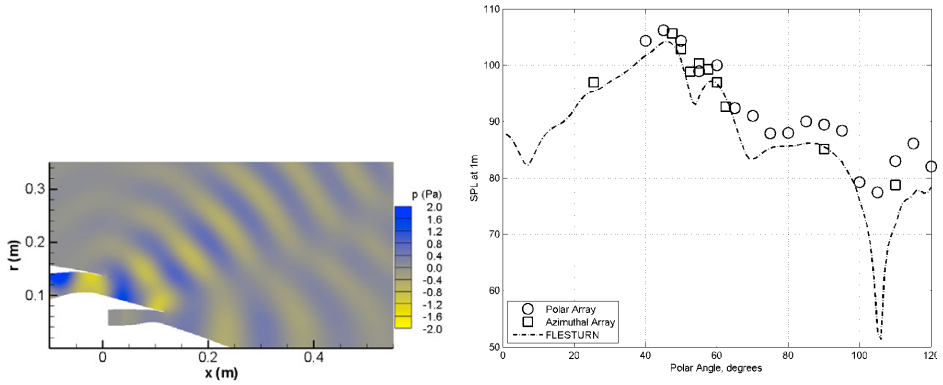

Figure 9: a) Pressure field for the m=0, n=1 mode with GTS, b) far-field SPL distribution (without GTA) for the m=0 mode at f=4056Hz, static approach (2 radial modes cut-on).

Figure 10a shows the pressure field for the m=8 target mode computed for the short cowl at 3810 Hz and the static cutback condition. Again a convective instability is apparent. This is indeed the K-H instability as confirmed by the parameters obtained through a similar simple analysis to the previous case as well as by the calculated Strouhal number distribution along the shear layer. There occured values of the Strouhal number that fell in the unstable region [1]. The pressure pattern indicates that the target mode radiates really away from the engine axis (above 90^o). The far-field directivity is compared with the measured data in Fig. 10b. It is evident that the far-field SPLs were under predicted up to about 80^o, and the agreement is reasonably good beyond this point. This case was one of the computed cases for which the TVA level was below 10 dB (see Table 1). Although this level shows the target mode was generated within the duct with reasonable dominancy, the measured overall far-field levels could be well under the influence of the propagating non-target modes which contribute to radiation in different directions, partially causing the observed discrepancies in the comparison. Another factor for the discrepancies could be the azimuthal mode broadening phenomenon detected in the far-field, which was attributed to a possible existence of asymmetry in the flow through the ducts or external jet flow [20].

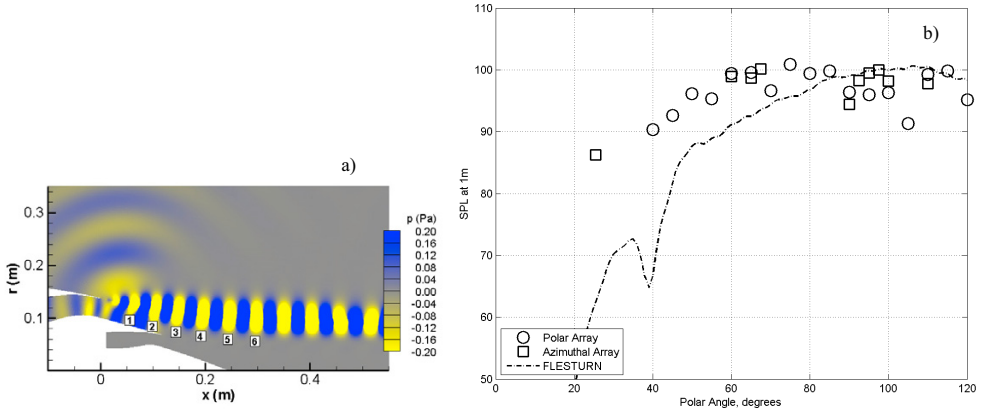

Figure 10: a) Pressure field for the m=8, n=1 mode at static cutback, f=3810 Hz. b) SPL distribution (1 rad. mode).

4.2. Long cowl configuration

Similar to the short cowl configuration, the long cowl measurements were made at four different flow conditions. All the FLESTURN acoustic computations for this case were also done with unit pascal amplitude and no phase differences between the cut-on radial modes at a given target azimuthal mode. During the post-processing of the far-field results, the radial modes were scaled and phase shifted with their actual in-duct measured complex mode amplitude data. Table 4 summarizes the presented long cowl cases.

Table 4: Long cowl acoustic cases.

Long cowl case 7	**TP**	**Freq, Hz**	***m***	**#radial modes**	**TVA, dB**
Static approach	50	4168.75	8	1	14.0
		7107.5	4	3	19.8
Static cutback	54	9843.75	5	4	9.4

Figure 11a and 11b show the far-field SPL comparisons for the long cowl m=8 mode at 4168.75 Hz and m=4 mode at 7107.5 Hz, both at the static approach condition. The in-duct TVA levels for these modes were 14 dB and 19.8 dB, respectively. Similar to some of the previous flow cases, the K-H instability developed for both cases. It is evident from Fig. 11a that the m=8 mode radiates mainly to very high angles (peak above 90 deg). The agreement between the computations and the measurements is confined in a very narrow range despite the good in-duct TVA level this mode had. The discrepancy pattern seen in the far-field comparison for this case is quite similar to that of the short cowl m=8 static cutback case (Fig. 10b). Similar reasoning can be given here for the discrepancies. As opposed to the m=8 mode at 4168.75 Hz, the far-field SPLs for the m=4 mode at 7107.5 Hz was computed for a large range of angles with a very good agreement with the measured far-field levels as evident from Fig. 11b. It may be useful to note that the main radiation direction for the latter is well below 90^o, while it was above 90^o for the former.

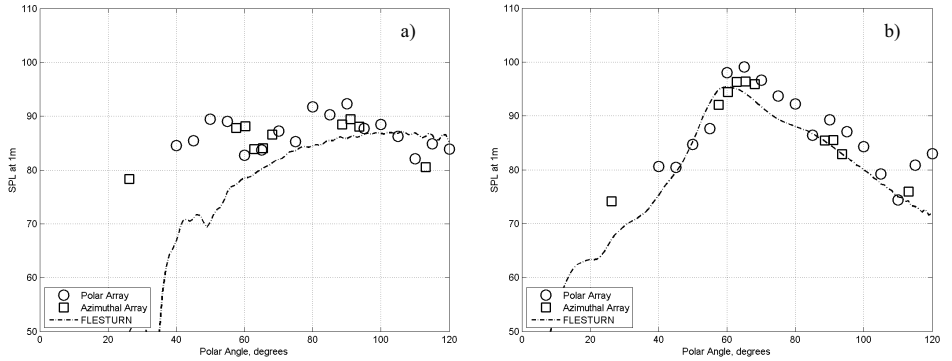

Figure 11: Far-field SPL at static approach, a) m=8, n=1 mode at f=4168.75 Hz, b) m=4, n=1 mode at f=7107.5 Hz.

The acoustic field for the first radial mode of the computed long cowl m=5 target mode at the static cutback condition and a frequency of 9843 Hz is shown in Fig. 12a. The in-duct TVA level was 9.4 dB for this target mode. It is evident from this figure that the K-H instability wave also appears for this case trailing the long cowl lip along the shear layer. The computed momentum thickness based Strouhal number was again within the unstable range, according to Michalke's results for round jets [1]. The K-H instability waves, however, remained bounded as in the previous cases, and the far-field radiation was not affected. A Kirchhoff-surface independency and a mesh independency study were also conducted for this case. It was found that the employed mesh and the Kirchhoff surface placements were sufficient to yield Kirchhoff surface and mesh independent results. For spatial brevity no results regarding these studies are shown here. The computed far-field SPLs agree with the measured data reasonably well, as illustrated in Fig. 12b. Again here the main radiation direction is below 90^o.

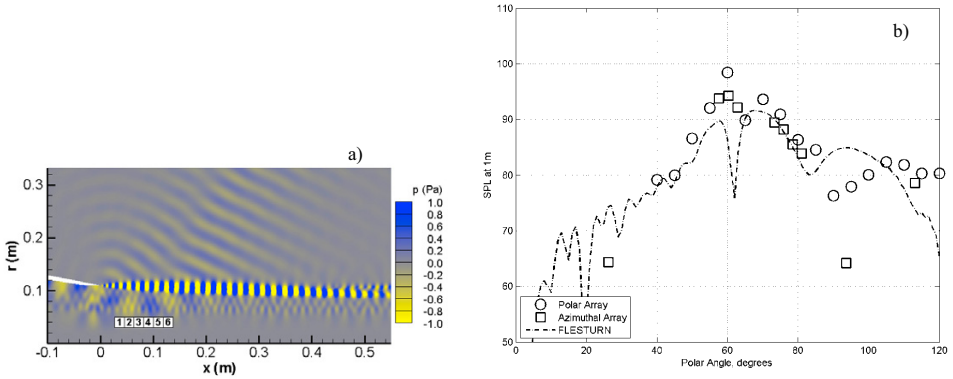

Figure 12: a) Pressure field for the m=5, n=1 mode at static cutback, f=9843 Hz, b) far-field SPL (4 rad. modes).

5. Concluding remarks

This paper has presented a short description of the frequency-domain LEE solver FLESTURN for predicting aft noise radiation through turbofan engine ducting systems and the sheared jet exhausts issuing from the nozzles. The code was developed within the framework of EC sponsored FP6 project TURNEX, which also acquired experimental data for radiation from two scale exhaust models, a ¾ short cowl and a long cowl (buried nozzle).

For the validation of the solver certain test points from these data measured at no flow, static approach and static cutback flow conditions were selected such that the target azimuthal mode level measured with an azimuthal far-field array (FFA) was not significantly lower than the other mode levels.

At some of the test conditions, the computed results clearly contained spatial instability waves along the bypass shear layer. These instability waves were demonstrated to be of the K-H type, i.e. convective in nature, by extracting the phase velocity information from the computed pressure contours and comparing with approximate theoretical phase velocity values. Also the momentum thickness based Strouhal number values were computed and compared with the theoretical stability criterion of Michalke [1]. Additional verification was provided by the close-up views of these waves revealing no radiation to the far field, typical of convective instabilities. Additional verification was provided by the close-up views of these waves revealing no radiation to the far field, typical of convective instabilities. Moreover, instability waves disappeared when the gradient terms were excluded from the LEE, again as was expected. The spatial instabilities were captured in the present solutions naturally, that is no explicit form for the wavenumber distribution was enforced in solving the equations; the independent variables are assumed of the form $\mathbf{q}(\mathbf{x},\omega)$ where $\mathbf{q}$ is complex and this therefore embodies all spatial wavenumbers (within grid resolution limits).

The computed far-field results were compared with the FFA overall tone data and good agreement both in terms of the levels and directivity pattern was usually obtained in the cases in which the FFA tone data was dominated by the target mode (high TVA levels), and only reasonable agreement was obtained in terms of the overall shape and level of the directivity pattern in the other cases. It is interesting to note that good agreement was usually obtained for the flow cases in which the main radiation direction was significantly below 90^o. From a previous appraisal of the experimental data, the appearance of stronger non-target modes in the far-field for some cases was attributed to the possibility of mode scattering phenomenon due to flow asymmetry in the ducts or external jet flow [20]. In addition, although it can be seen that the in-duct TVA levels were normally 10 dB or greater for most cases, it is quite possible that parts of the far-field directivity contained contributions from azimuthal modes other than the target mode. It is therefore our intention in future work to include the significant non-target modes in an attempt to improve the agreement between measurement and our predictions.

It is emphasized that the agreement between far-field measured and numerical solutions has been achieved in terms of *absolute* levels, based on the in-duct measured absolute azimuthal/radial mode levels used to 'drive' the FLESTURN solutions. The agreement strongly suggests that, at least for this range of mean flows and acoustic

conditions, the physical aeroacoustic radiation processes have been fully captured through the frequency-domain solutions to the linearised Euler equations.

Acknowledgements

This work was funded by the EC through the TURNEX project (Tech. Officer: Daniel Chiron).

References

[1] A. Michalke, "Survey on jet instability theory," *Progress in Aerospace Sciences*, 21(1984) 159-199.
[2] A. Agarwal, P. J. Morris, R. Mani, "The calculation of sound propagation in nonuniform flows: Suppression of instability waves," *AIAA Journal*, **42**(1) (2004), pp. 80-88.
[3] J. Kok, "Computation of sound radiation from cylindrical ducts with jets using a high-order finite-volume method," AIAA Paper 2007-3489, 13th AIAA/CEAS Aeroacoustics Conference, Rome, Italy (May 2007).
[4] J. Manera, B. Schiltz, R. Leneveu, S. Caro, J. Jacqmot, S. Rienstra, "Kelvin-Helmholtz instabilities occurring at a nacelle exhaust," AIAA Paper 2008-2883, 14th AIAA/CEAS Aeroacoustics Conference, Vancouver, Canada (May 2008).
[5] X. Zhang, X. X. Chen, C.L. Morfey, P. A. Nelson, "Computation of spinning modal radiation from an unflanged duct," *AIAA Journal*, **42**(9) (2004) 1795-1801.
[6] C. Bogey, C. Bailly, D. Juve, "Computation of Flow Noise Using Source Terms in Linearized Euler's Equations," AIAA *Journal*, **40**(2) (Feb. 2002), pp. 235-243.
[7] B. J. Tester, G. Gabard, Y. Özyörük, "Influence of mean flow gradients on fan exhaust noise prediction," AIAA Paper 2008-2825, 14th AIAA/CEAS Aeroacoustics Conference, Vancouver, Canada (May 2008).
[8] Y. Zhao, P. J. Morris, "The prediction of fan exhaust noise propagation," AIAA Paper 2005-2815, 11th AIAA/CEAS Aeroacoustics Conference, Monterey, California (May 2005).
[9] Y. Özyörük, "Numerical prediction of aft radiation of turbofan tones through exhaust jets," *Journal of Sound and Vibration*, **325** (1-2), August 2009, pp. 122-144.
[10] Y. Özyörük, E. Dizemen, A. Aktürk, S. Kaya, "A Frequency Domain Linearized Euler Solver for Turbomachinery Noise Propagation and Radiation," AIAA Paper 2007-3521, 13th AIAA/CEAS Aeroacoustics Conference, Rome, Italy (May 2007).
[11] http://mumps.enseeiht.fr/, MUMPS: a MUltifrontal Massively Parallel sparse direct Solver.
[12] P.R. Amestoy, I.S. Duff, J.-Y.L. L'Excellent, "Multifrontal parallel distributed symmetric and unsymmetric solvers," *Comput. Methods in Appl. Mech. Eng.* **184** (2000) 501-520.
[13] R. M. Munt, "The interaction of sound with a subsonic jet issuing from a semi-infinite cylindrical pipe," *Journal of Fluid Mechanics*, **4** (1977), pp. 609-640.
[14] G. Gabard, R. J. Astley, "Theoretical models for sound radiation from annular jet pipers: far- and near-field solutions," *Journal of Fluid Mechanics*, **549** (2006) 315-342.
[15] A. Demir, S. Rienstra, "Sound radiation from an annular duct with jet flow and a lined centerbody," AIAA paper 2006-2718, 12th AIAA Aeroacoustics Conference, Cambridge, MA (May 2006).
[16] Q.F. Hu, "A perfectly matched layer absorbing boundary condition for linearized Euler equations with a non-uniform mean flow," *Journal of Computational Physics*, **208** (2005), pp. 469-492.
[17] M. K. Myers, "On the acoustic boundary condition in the presence of flow," *Journal of Sound and Vibration*, **71**(3) (1980), pp. 429-434.
[18] C.K.W. Tam, J.C. Webb, "Dispersion-relation-preserving finite difference schemes for computational acoustics," *Journal of Computational Physics* **107** (1993) 262-281.
[19] F. Arnold, U. Tapken, R. Bauers, and J. Zillmann, "Turbomachinery Exhaust Noise Radiation Experiments – Part 1: Polar Directivity Measurements," AIAA Paper 2008-2857, 14th CEAS/AIAA Aeroacoustics Conference, Vancouver, Canada (May 2008).
[20] U. Tapken, R. Bauers, F. Arnold, J. Zillmann, "Turbomachinery Exhaust Noise Radiation Experiments – Part 2: In-duct and Far-Field Mode Analysis", AIAA Paper 2008-2858, 14th CEAS/AIAA Aeroacoustics Conference, Vancouver, Canada (May 2008).
[21] C.J. Moore, "The role of shear-layer instability waves in jet exhaust noise," J. Fluid Mech, **80**, part2, (1977), pp. 321-367.